Journal of Alloys and Compounds 519 (2012) 149–155

Contents lists available at SciVerse ScienceDirect

Journal of Alloys and Compounds

journal homepage: www.elsevier.com/locate/jallcom

Luminescent properties of yellowish orange $Y_3Al_{5-x}Si_xO_{12-x}N_x$:Ce phosphors and their applications in warm white light-emitting diodes

Xiaojun Wang[a], Guohong Zhou[b], Hailong Zhang[b], Huili Li[a,*], Zhejuan Zhang[a], Zhuo Sun[a]

[a] Engineering Research Center for Nanophotonics and Advanced Instrument, Ministry of Education, Department of Physics, East China Normal University, Shanghai 200062, China
[b] Structural Ceramics Center, Shanghai Institute of Ceramics, Chinese Academy of Sciences, Shanghai 200050, China

ARTICLE INFO

Article history:
Received 28 October 2011
Received in revised form
29 December 2011
Accepted 29 December 2011
Available online 5 January 2012

Keywords:
$Y_3Al_5O_{12}:Ce^{3+}$
Si_3N_4
Phosphor
Color rendering index
White light-emitting diodes

ABSTRACT

This paper reports a low-cost yellow-orange emitting $Y_3Al_{5-x}Si_xO_{12-x}N_x:Ce^{3+}$ phosphor with excellent color rendering for warm white LEDs. It was synthesized by a simple gas pressure sintering (GPS). The effect of Si^{4+}—N^{3-} incorporation on the optical properties of $Y_3Al_5O_{12}:Ce^{3+}$ phosphor was investigated. The addition of Si_3N_4 leads to an obvious shift of its emission spectra toward the red region and an increase of FWHM accompanying a significant decrease of photoluminescent intensity, which is assigned to incorporation of N^{3-} in Ce^{3+} nearest neighbor coordination. Adding nanosized amorphous Si_3N_4 or flux can greatly improve the emission intensity of $Y_{2.925}Ce_{0.075}Al_{5-x}Si_xO_{12-x}N_x$ phosphor. Finally, the white LED flat lamp with a CRI as high as 83, luminous efficiency of 65 lm/W, and CCT of about 3700 K is successfully realized by using a single oxynitride phosphor combined with a blue LED chip, which is acceptable for general indoor illuminations to replace fluorescent or incandescent lamps.

1. Introduction

The development of InGaN-based light-emitting diodes (LEDs) has led to a rapid growth in the solid-state lighting industry because they couple to phosphors that convert a part of their emission to yellow light to generate white LEDs [1–3]. Among these phosphors, cerium-doped yttrium aluminum garnet ($Y_3Al_5O_{12}:Ce^{3+}$, YAG:Ce) is the best choice. As excited by the blue radiation, it shows an efficient broad luminescence in yellow region, high quantum efficiency (QE, >90%), high chemical and photochemical stability [4–8]. Recent improvement of internal QE and light extraction of InGaN LEDs has resulted in record luminous efficiency of YAG:Ce phosphor based white LEDs far beyond 100 lm/W which is higher than that of compact fluorescent lamps (CFLs) and comparable to that of linear fluorescent lamps (LFLs) [9–11]. However, other requirements, such as the correlated color temperature (CCT) and color rendering index (CRI), need to be optimized before white LEDs can extensively replace fluorescent or incandescent light sources due to lack of red component in the emission spectra of YAG:Ce phosphors. The highest efficacy white LEDs have CCTs in excess of 5000 K (cool white and daylight LEDs), making them less acceptable as replacements for incandescent and halogen lamps that have CCTs of 2500–3200 K. The corresponding CRIs are less than 75, which is far below CRIs of 100 for incandescent and halogen lamps and 82–85 for CFLs [11]. Therefore, in order to achieve lower CCTs and higher CRIs, the red phosphors are required to compensate for the spectral deficiencies of standard phosphor converted white LEDs (pc-WLEDs).

Recently, lots of significant effort has been put for shifting the emission spectrum of YAG:Ce into the red spectral region either by codoping with other rare-earth ions (Pr^{3+}) or by substituting Y^{3+} by other cations (especially by Tb^{3+} and Gd^{3+}) [12–17]. In addition, some efficient nitride-based red phosphors such as (Ca, Sr, Ba)$_2Si_5N_8:Eu^{2+}$ [18,19], α-SiAlON:Eu^{2+} [20,21], $CaAlSiN_3:Eu^{2+}$ [22] and $SrAlSiN_3:Eu^{2+}$ [23] have been developed and met some of the spectral requirements for general indoor lighting. However, the difficulty in synthesis and stability of nitride-based phosphors still remains a big challenge for chemists and material scientists.

It is well known that the position of Ce^{3+} 5d energy levels depends on the nephelauxetic effect (covalency), crystal-field splitting and the Stokes shift [24]. Therefore, for garnet-based phosphors, a further red shift of the Ce^{3+} emission spectrum can also be achieved by increasing covalency, for instance, by substitution of Al^{3+} by Mg^{2+}—Si^{4+} pairs on the octahedral and tetrahedral sites, respectively [25,26]. However, this redshift comes along with a decrease in phosphor emission intensity and high temperature quenching. Recently, Setlur and co-workers found that a partial replacement of Al^{3+} (tetrahedral)—O^{2-} with Si^{4+}—N^{3-} in YAG:Ce led to an additional red component in the emission spectra due to incorporating ligands with a lower electronegativity and increasing covalent character and crystal-field strength. But

* Corresponding author. Tel.: +86 21 62235465; fax: +86 21 62234321.
E-mail address: hlli@phy.ecnu.edu.cn (H. Li).

0925-8388/$ – see front matter © 2012 Elsevier B.V. All rights reserved.
doi:10.1016/j.jallcom.2011.12.158

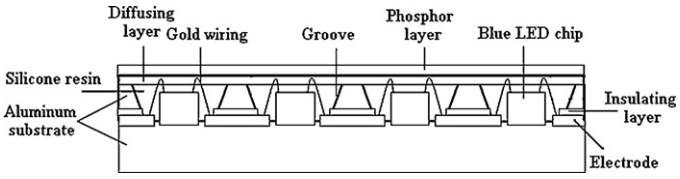

Fig. 1. Schematic of white LED flat source.

a stronger thermal quenching still existed compared to nonsubstituted YAG:Ce phosphors. The mechanism for this quenching was discussed [11,27]. These luminescent results were significantly different from those in a prior literature report on a blueshift in the emission spectra caused by Si^{4+}—N^{3-} incorporation in YAG:Ce phosphors [28], but similar to reports in the patent literatures [27,29,30].

The incorporation of Si^{4+}—N^{3-} into YAG:Ce in the previous reports [11,27–30] was achieved by longtime high temperature sintering repeatedly under a normal atmosphere, which is high energy consumption and high cost. In our present work, for an effort to increase the substitution of Si^{4+}—N^{3-} for Al^{3+}—O^{2-} and improve the color properties of YAG:Ce phosphor, we adopted a gas-pressure sintering (GPS) process in preparing Si_3N_4-doped YAG:Ce phosphors and reported Si_3N_4 concentration-dependent structure and luminescent properties. In order to improve the emission intensity, the influence of nano-sized Si_3N_4 and different flux on optical properties was investigated. Finally, warm-white LED flat lamps were made by using the optimized oxynitride garnet phosphors combined with InGaN-based blue chips (λ_{max} = 445–450 nm) and their electroluminescent (EL) characteristics were also evaluated.

2. Experimental

2.1. Source materials

Si_3N_4-doped YAG:Ce phosphors were prepared by a conventional solid-state reaction method. Y_2O_3 (99.999%), nanosized α-Al_2O_3 (99.99%, average particle size: 20 nm), CeO_2 (99.999%), α-Si_3N_4 (SN-E10, α content: >95%, oxygen content: <2.0%, SSA: 9–13 m^2/g), nanosized Si_3N_4 (>99%, amorphous, SSA: 50 m^2/g), LiF (analytical grade), HBO_3 (analytical grade), and NH_4F (analytical grade) were used as starting materials in the present work. Si^{4+} in these compositions was provided by α-Si_3N_4 or nanosized Si_3N_4, giving a slight excess of N^{3-}, and LiF or HBO_3 or NH_4F was added as a fluxing agent to improve the efficiency of phosphor.

2.2. Synthesis of undoped and Si_3N_4-doped YAG:Ce phosphors

Oxynitride phosphors with compositions of $Y_{2.925}Ce_{0.075}Al_{5-x}Si_xO_{12-x}N_x$ (x = 0.00–0.60) were prepared by weighing, mixing, and grinding the appropriate amount of starting materials in a mortar by hand. Subsequently, they were fired in an alumina crucible at 1400–1500 °C for 2–6 h in gas-pressure sintering furnace with a graphite heater under 0.5–1.0 MPa N_2 atmosphere. After firing, samples were cooled to room temperature (RT) in the furnace and were ground again with an agate mortar for further measurements.

2.3. Fabrication of white LED flat lamps

White LED flat lamps with special construction, as shown in Fig. 1, were fabricated using as-prepared oxynitride phosphors. The primary light source is the commercially available InGaN-based semiconductor blue LED chips. They were fixed on the grooves in the aluminum substrate and connected to electrodes. The grooves were filled with the transparent silicone resin till the blue LED chips were covered. A layer of diffusing material was coated on the transparent silicone resin in order to make the emitting light homogeneous distribution. Then, the synthesized oxynitride phosphors with the same content were dispersed into the transparent silicone resin, poured to coat the diffusing layer. Finally, a white LED flat lamp was formed.

2.4. Structural and morphological characterization

X-ray powder diffraction (XRD) patterns of the prepared phosphors were recorded on a D8 ADVANCE X-ray diffractometer with the Cu Kα radiation at 40 kV and 40 mA. The morphology was observed by a field emission scanning electron microscope (FESEM, Hitachi S-4800). The element compositions were measured by an energy dispersive spectroscopy (EDS) on the FESEM.

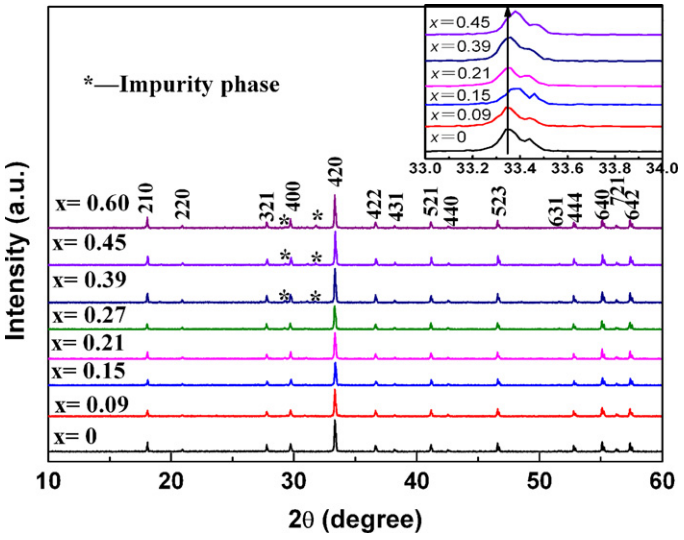

Fig. 2. XRD patterns of $Y_{2.925}Ce_{0.075}Al_{5-x}Si_xO_{12-x}N_x$ phosphors.

2.5. Optical measurements

The photoluminescence (PL) spectra and quantum yield of undoped and Si_3N_4-doped phosphors were examined at RT by a fluorescence spectrophotometer (Horiba Jobin Yvon, FluoroMax-4) with a 150 W Xe lamp as an excitation source. The quantum yield was estimated using an integrating sphere unit (Horiba Jobin Yvon, F-3029). The samples were placed in the integrating sphere and excited by a monochromatic source with a wavelength of 445 nm, and were determined by using the following equation:

$$\varphi = \frac{E_c - E_a}{L_a - L_c} \quad (1)$$

where E_c is the integrated luminescence intensity of the sample caused by 445 nm excitation, and E_a is the integrated luminescence intensity from an empty integrating sphere (only a blank). L_a is the integrated excitation profile from an empty integrating sphere (without the sample, only a blank), and L_c is the integrated excitation profile from the sample. Optical properties such as luminous efficiency, CRI, CCT, and the Commission Internationale de l'Eclairage (CIE) color coordinates of as-fabricated white LEDs were investigated by a UV–Vis–near IR spectrophoto colorimeter (PMS-80) with an integrating sphere under a forward-bias current of 20 mA at RT.

3. Results and discussion

3.1. Effect of α-Si_3N_4 on the structure and luminescence properties of YAG:Ce^{3+}

Fig. 2 shows the XRD patterns of YAG:Ce^{3+} phosphors with different amounts of α-Si_3N_4. It can be seen that the as-synthesized samples with $x \leq 0.27$ show a pure phase of YAG. All the diffraction peaks correspond to the cubic garnet crystal structure. But an additional impurity phase is found when x increases to 0.39, and its relative content gradually increases with the x increasing from 0.39 to 0.6, which suggests that the solubility limit of Si^{4+}—N^{3-} in YAG is less than 0.39, corresponding to the nominal composition of $Y_{2.925}Ce_{0.075}Al_{4.61}Si_{0.39}O_{11.61}N_{0.39}$. The results are similar to those in the previous experiments [11,31] which estimated that Si^{4+} can replace ~12% of the tetrahedral Al^{3+} sites in YAG when N^{3-} is the charge compensating ion, giving a garnet composition of $Y_3Al_{4.65}Si_{0.35}O_{11.65}N_{0.35}$. Of course, different processing conditions such as firing temperature, atmosphere, pressure, starting material, flux, holding time could have some effects on the solubility limit of Si^{4+}—N^{3-}. Additionally, compared to the undoped sample, the addition of α-Si_3N_4 leads to an obvious shift of diffraction peaks to the large angle (see the inset in Fig. 2), which indicates lattice shrinkage of YAG caused by the substitution of the shorter tetrahedral Si^{4+}—N^{3-} bonds (1.685–1.76 Å in α-Si_3N_4) for the longer tetrahedral

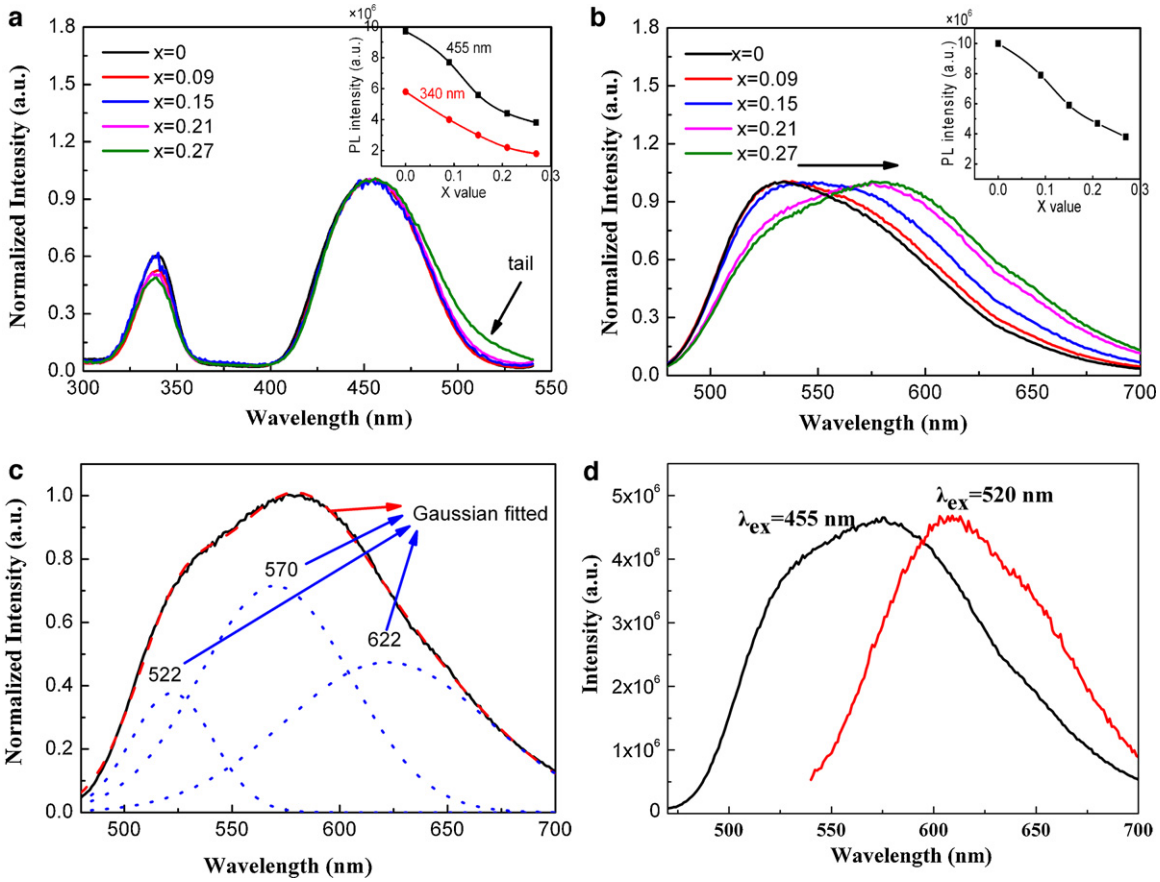

Fig. 3. Normalized excitation (a) and emission spectra (b) of $Y_{2.925}Ce_{0.075}Al_{5-x}Si_xO_{12-x}N_x$ phosphors; the inset presents PL intensity as a function of x value; (c) the Gaussian fitted (dashed) and decomposed components (dotted) of the emission spectrum for $Y_{2.925}Ce_{0.075}Al_{4.73}Si_{0.27}O_{11.73}N_{0.27}$; (d) emission spectra for $Y_{2.925}Ce_{0.075}Al_{4.73}Si_{0.27}O_{11.73}N_{0.27}$ under different excitation wavelength.

Al^{3+}—O^{2-} bonds (1.761 Å) [11] as well as the smaller size of Si^{4+} (0.26 Å) for the larger size of Al^{3+} (0.39 Å) [28].

The excitation and emission spectra of YAG:Ce^{3+} phosphors with different amounts of α-Si_3N_4 are given in Fig. 3a and b. All the excitation spectra consist of two major peaks at 340 and 455 nm, which are assigned to the characteristic $4f^1 \rightarrow 5d^1$ transition of Ce^{3+} ions [32]. Adding Si^{4+}—N^{3-} to YAG:Ce^{3+} does not change positions of two excitation bands but a low-energy tail in the blue-green region is observed for samples consisting of high content Si^{4+}—N^{3-} (i.e. $x = 0.27$), as seen in Fig. 3a. It suggests that an additional Ce^{3+} site appears due to incorporation of N^{3-} into its nearest neighbor coordination. Under the excitation of 455 nm, $Y_{2.925}Ce_{0.075}Al_{5-x}Si_xO_{12-x}N_x$ shows a typical $5d^1 \rightarrow 4f^1$ broad emission of Ce^{3+} (Fig. 3b). The emission band gradually red-shifts and becomes broader with x increasing from 0 to 0.27. The wavelength of the highest emission intensity shifts from 533 to 583 nm and the corresponding full width at half-maximum (FWHM) increases from 105 to 136 nm. The samples with $x = 0.21$ and 0.27 consist of a strong red spectral component, which make it possible for single pc-WLED with CCT less than 4000 K and CRI greater than 80 [11,27,29,30]. After Gaussian deconvolution, the broad emission band for $Y_{2.925}Ce_{0.075}Al_{4.73}Si_{0.27}O_{11.73}N_{0.27}$ can be well decomposed into three components centered at about 522, 570 and 622 nm (Fig. 3c). The two higher energy splitting bands with an energy difference of about 1600 cm^{-1} should come from the splitting of the $4f^1$ ground sate configuration of the Ce^{3+} ion (lower than the normal energy difference of about 2000 cm^{-1} between $^2F_{7/2}$ and $^2F_{5/2}$ levels) [24]. Another red emission band with lower energy should be assigned to an additional Ce^{3+} site with N^{3-} into its nearest neighbor coordination, which can be confirmed by emission spectra in Fig. 3d. Under green excitation of 520 nm (the tail in Fig. 3a), $Y_{2.925}Ce_{0.075}Al_{4.73}Si_{0.27}O_{11.73}N_{0.27}$ exhibits a low-energy red emission with a maximum at 610–620 nm. The corresponding Stokes shift is about ~3100 cm^{-1}, larger than that of ~2400 cm^{-1} for typical aluminate garnets [33].

All the above redshift phenomena are similar to previous reports [11,27–30], and likely due to a shift in the Ce^{3+} $5d^1$ centroid to both of the higher covalency and polarizability of Ce^{3+}—N^{3-} bonds versus Ce^{3+}—O^{2-} bonds. The incorporation of N^{3-} anions with a lower electronegativity ($\chi(N) \approx 3.0$) compared to O^{2-} ($\chi(O) \approx 3.4$) would lower the energy of the $5d^1$ excited levels and lead to redder emission. In addition, the difference between the ionic size of Si^{4+} and with Al^{3+} ion also influences the structural symmetry surrounding Ce^{3+} ions. That is, the cubic structure of YAG host will be distorted by the incorporation of Si^{4+} ions, which lowers the symmetry of the YAG host crystal and increases the crystal field strength.

Except for the redshift in the emission position, the addition of Si^{4+}—N^{3-} also leads to a rapid reduction in PL intensity (see insets in Fig. 3a and b). This reduction should come from a decrease of quantum yield of phosphor with x increasing from 0 to 0.27 (shown in Table 1), a variation in morphology and size of particle and an increase in Stokes shift. Fig. 4 shows SEM images of phosphor doped with different content α-Si_3N_4. The undoped YAG:Ce^{3+} powders crystallize well and give near-spherical morphology. The particle size locates at 3–15 μm. After α-Si_3N_4 adds to YAG host, the particle size sharply decreases to about 1 μm. Some irregular aggregates happen. Increasing α-Si_3N_4 content causes more serious aggregates and irregular morphology, finally, reduces PL intensity

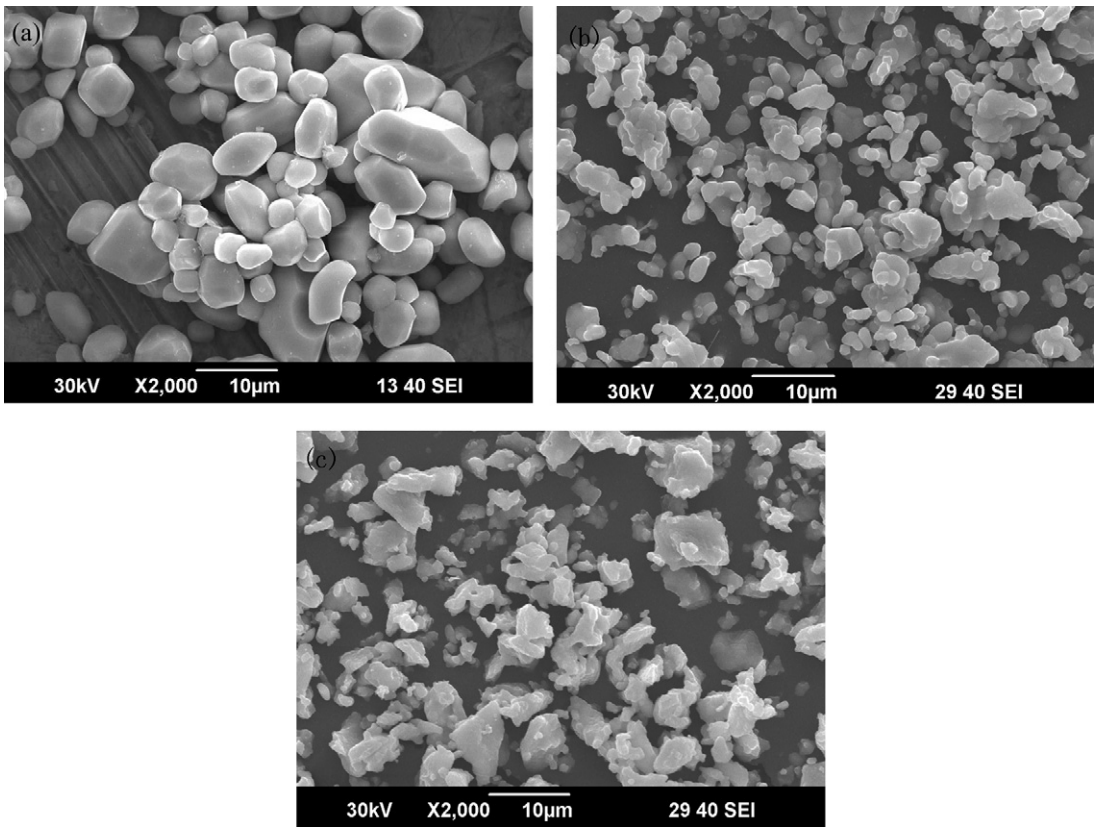

Fig. 4. SEM images of $Y_{2.925}Ce_{0.075}Al_{5-x}Si_xO_{12-x}N_x$ phosphors: (a) $x = 0$; (b) $x = 0.09$; and (c) $x = 0.21$.

Table 1
Normalized quantum yields of $Y_{2.925}Ce_{0.075}Al_{5-x}Si_xO_{12-x}N_x$ phosphors.

x value	Normalized quantum yield (%)
0	100.00
0.09	68.34
0.15	54.66
0.21	45.62
0.29	32.92

of phosphors. On the other hand, under the same excitation wavelength of 455 nm, the emission spectra of phosphors doped with α-Si_3N_4 present an obvious redshift and an increase of the Stokes shift (Fig. 3b), which can also lead to the reduction of PL intensity.

The element components of as-prepared $Y_{2.925}Ce_{0.075}Al_{5-x}Si_xO_{12-x}N_x$ phosphors were identified by EDS attached to FESEM, as shown in Table 2. One can find that the elements of Si and N are obviously detected in Si_3N_4-doped samples. Moreover, their contents increase with α-Si_3N_4 dopant, again indicating that Si_3N_4 were successfully incorporated into YAG host. These results are in agreement with XRD and PL spectra in Figs. 2 and 3.

Table 2
The element components of $Y_{2.925}Ce_{0.075}Al_{5-x}Si_xO_{12-x}N_x$ phosphors.

x value	Element content (at.%)	
	Si	N
0	0	0
0.09	0.2	8.15
0.21	0.41	8.62

3.2. Optical properties of white LED flat sources fabricated by using as-prepared $Y_{2.925}Ce_{0.075}Al_{5-x}Si_xO_{12-x}N_x$ phosphors

Five white LED flat lamps with special construction shown in Fig. 1 were fabricated by using as-prepared oxynitride phosphors combined with the blue InGaN chips. The dominant wavelength of the used blue LED chip varies from 445 to 450 nm. The emission spectra of these white LED flat lamps are shown in Fig. 5. By the addition of α-Si_3N_4 to YAG host lattice, the red emission intensity

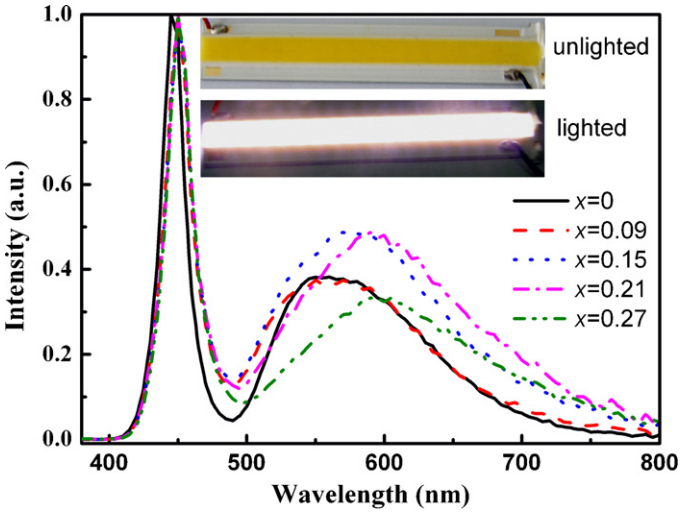

Fig. 5. Normalized emission spectra of the high CRI white LED flat lamps fabricated by using $Y_{2.925}Ce_{0.075}Al_{5-x}Si_xO_{12-x}N_x$ phosphors combined with InGaN chips, operated at a forward-bias current of 20 mA at RT. Inset is photograph of a typical white LED flat lamp.

Table 3
Optical properties of the white LED flat lamps fabricated by using as-prepared $Y_{2.925}Ce_{0.075}Al_{5-x}Si_xO_{12-x}N_x$ phosphors combined with blue InGaN chips.

x value	CIE coordinates		CCT (K)	CRI	Luminous efficacy (lm/W)
	x	*y*			
0	0.3185	0.3606	6070	69	89
0.09	0.3075	0.2963	7200	83	79
0.15	0.3383	0.3186	5200	85	55
0.21	0.3489	0.2991	4500	88	42
0.27	0.3236	0.2526	6500	82	41

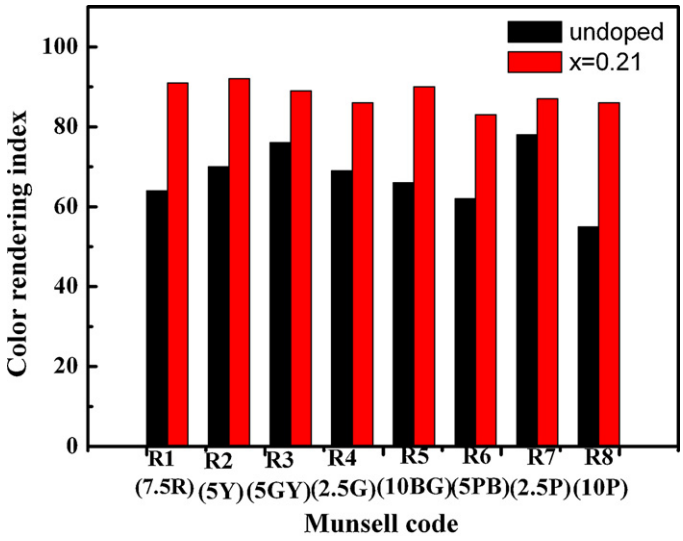

Fig. 6. CRI values from R1 to R8 of the fabricated white LED lamps using undoped and Si_3N_4 doped phosphor ($x = 0.21$).

around at 600 nm is greatly improved. The intense warm white light emission can be observed under a forward-bias current of 20 mA, see the inset in Fig. 5.

Table 3 presents the chromaticity coordinates, the CCTs, the CRI values and the luminous efficacies of the fabricated lamps. The samples doped with α-Si_3N_4 obviously give high CRI values which increase with α-Si_3N_4 content and are higher than 80 for all lamps with different oxynitride phosphors. Especially, CRI reaches 88 for sample with $x = 0.21$, which is much higher than 69 of undoped sample. Fig. 6 displays the CRIs of white LED lamps fabricated by using undoped and α-Si_3N_4-doped ($x = 0.21$) YAG:Ce^{3+} phosphors under a forward-bias current of 20 mA. The general CRI value is

Table 4
Special CRI values from R9 to R15 of as-fabricated white LED lamps doped with different α-Si_3N_4.

x value	R9	R10	R11	R12	R13	R14	R15
$x = 0$	0	39	65	36	65	90	55
$x = 0.21$	73	82	80	68	91	93	96

designated by the symbol Ra which is the average value of R1–R8. Numbers in parentheses indicate the Munsell hues in the Munsell color system [34]. In comparison with an undoped YAG:Ce-based white LED, the α-Si_3N_4-doped ($x = 0.21$) YAG:Ce-based white LED has higher values of R1 (7.5R) and R8 (10P) which are both related to red color. The special CRI values from R9 to R15 for undoped and α-Si_3N_4-doped ($x = 0.21$) YAG:Ce-based white LED lamps are shown in Table 4, which are not evaluated in calculating the general CRI value. We can see that these CRI values for YAG:Ce-based white LED lamp with $x = 0.21$ are also extremely high, which means that the color can be precisely reproduced for any color objects. Generally speaking, the white LED lamp with very high CRI value requires blending two or three even to four kinds of phosphors, which possibly leads to some variations in properties during lamp manufacturing. But the present outcome indicates that high CRI white LED lamp can also be realized by using a single phosphor with broad emission spectrum instead of phosphor blends.

On the other hand, the chromaticity coordinates and CCTs of white LED lamps are unsatisfactory even though their CRI values are excellent (Table 3). This is because that the concentration of phosphor in silicone resin is too low or the phosphor layer coated on the diffusing layer and blue chip is too thin, which results in high ratio of blue light emitted from the blue LED chip. These properties can be optimized in the future applications. In addition, it also can be seen that the luminous efficacy of white LED lamp markedly decreases from 89 to 41 lm/W with *x* (Si_3N_4 content) increasing from 0 to 0.27 (shown in Table 3). This is understandable because high Ra white LED lamp always accompany a decrease of the luminous efficacy which is caused by the decrease of PL intensity of phosphor. The low luminous efficacy of Si_3N_4-doped YAG:Ce-based white LED can be improved by optimizing the morphology, particle size and increasing quantum yield of the phosphor, which will be investigated further details in the following work.

3.3. *Effects of nano-sized Si_3N_4 and flux on the structure and luminescence properties of YAG:Ce^{3+}*

In a solid-state reaction, the use of nanosized powder and flux is a popular method to enhance the emission intensity of phosphors.

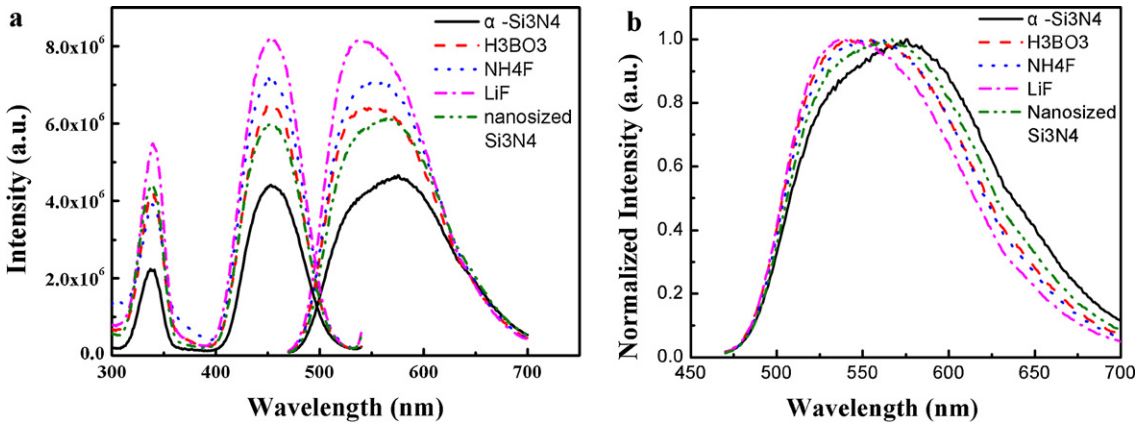

Fig. 7. Photoluminescence spectra (a) and normalized emission spectra (b) of $Y_{2.925}Ce_{0.075}Al_{4.79}Si_{0.21}O_{11.72}N_{0.21}$ phosphors with different kinds of Si_3N_4 and flux.

As the same purpose, we substitute nanosized amorphous Si_3N_4 for α-Si_3N_4 in $Y_{2.925}Ce_{0.075}Al_{4.79}Si_{0.21}O_{11.72}N_{0.21}$ phosphor and also add different kinds of flux with the intention of enhancing the emission efficiency of oxynitride phosphor. Fig. 7a shows the excitation and emission spectra of $Y_{2.925}Ce_{0.075}Al_{4.79}Si_{0.21}O_{11.72}N_{0.21}$ phosphor doped with different kinds of Si_3N_4 and flux. It is clear that the integrated excitation and emission intensity of oxynitride phosphor is greatly improved by the substitutuion of nanosized amorphous Si_3N_4 for α-Si_3N_4. The PL intensity increases further when the flux is added to oxynitride phosphor. The highest luminescence intensity is observed in the sample with LiF as a flux and is about 1.8 times higher than that of α-Si_3N_4-doped sample without flux. However, an obvious blueshift in the position of the maximum emission peak is observed with the substitution of nanosized amorphous Si_3N_4 for α-Si_3N_4 and the addition of flux from NH_4F, H_3BO_3 to LiF (Fig. 7b). Simultaneously, the corresponding FWHM slightly decreases from 129 to 112 nm which is still much broader than that of pure YAG:Ce^{3+} without Si_3N_4 (Fig. 3b).

In order to explain the above luminescent phenomena, the effects of additives on the crystal structure and morphology of YAG:Ce phosphors are investigated. Compared with the standard JCPDF card of $Y_3Al_5O_{12}$ (No. 79-1892), all the synthesized samples show a pure garnet phase and no impurity related to Si_3N_4 or flux is detected (Fig. 8), which indicates that flux or substitution has no obvious influence on the phase structure of the host. However, the diffraction intensity of samples consisting of nanosized amorphous Si_3N_4 or flux markedly increase compared with that of sample doped with α-Si_3N_4, suggesting that the crystallinity of particles is improved when nanosized amorphous Si_3N_4 or flux is added. This is can be further demonstrated by the following SEM morphologies in Fig. 9. After substitution of nanosized amorphous Si_3N_4 (Fig. 9b) for α-Si_3N_4 (Fig. 9a), the average particle size of phosphor evidently increases and gives relatively uniform, dispersive

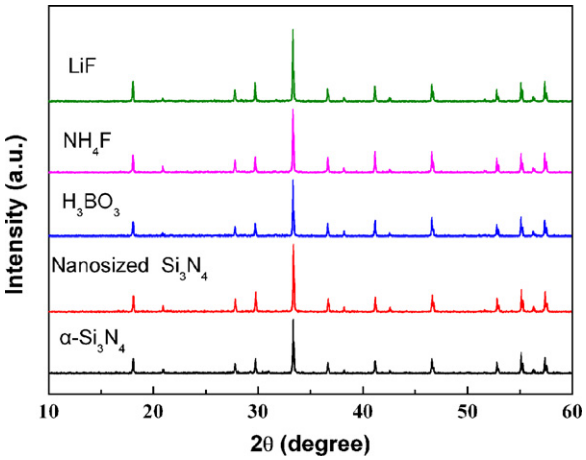

Fig. 8. XRD patterns of $Y_{2.925}Ce_{0.075}Al_{4.79}Si_{0.21}O_{11.72}N_{0.21}$ phosphors with different kinds of Si_3N_4 and flux.

morphology. When the flux of NH_4F is added (Fig. 9c), the crystallite size increases in further and the observed biggest single-crystal particles reach 10 μm. The aggregates caused by smaller particles disappear and the best morphology is exhibited. Generally, the crystallinity of phosphor is one of the important factors affecting the luminescence intensity, the better crystallinity, the better the optical property. Therefore, the enhancement of emission intensity of the phosphor is attributed to the improved crystallinity of particles, the narrower particle size distribution, and the better morphology when nanosized amorphous Si_3N_4 or flux is added, as shown in Fig. 7a.

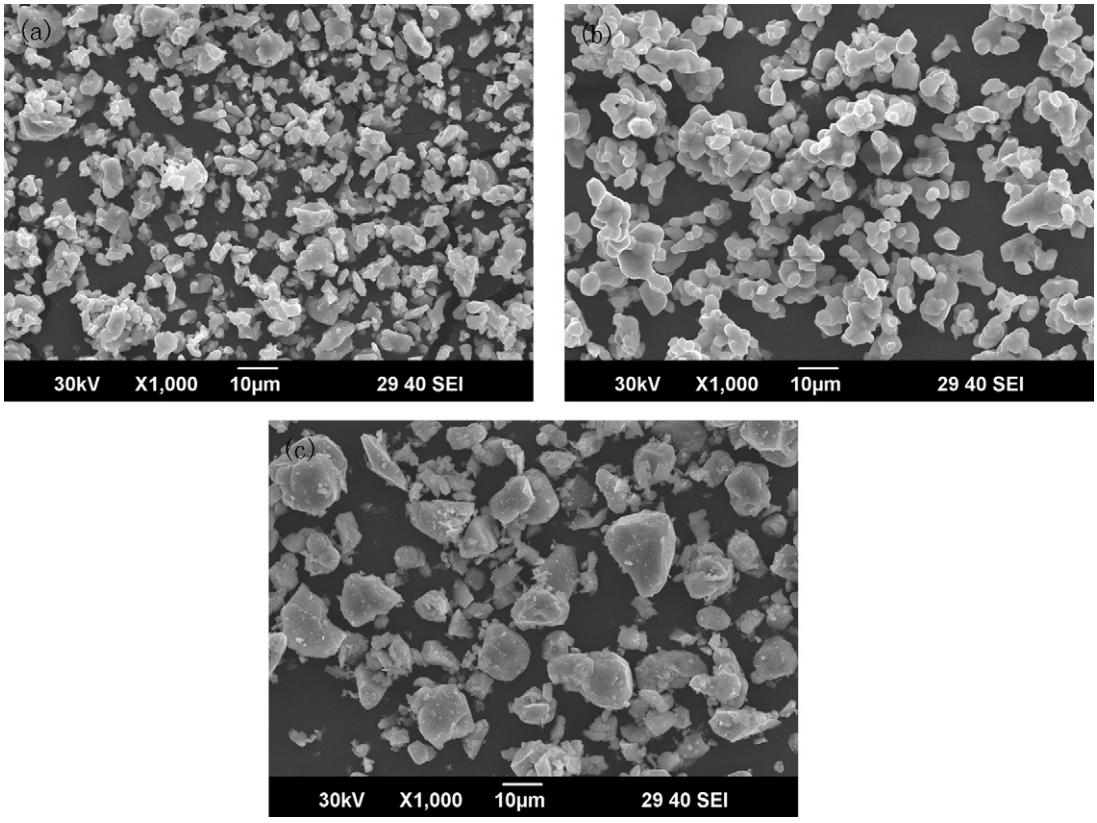

Fig. 9. SEM photos of $Y_{2.925}Ce_{0.075}Al_{4.79}Si_{0.21}O_{11.72}N_{0.21}$ phosphors doped with: (a) α-Si_3N_4; (b) nanosized amorphous Si_3N_4; and (c) NH_4F as a flux.

Table 5
Optical properties of white LED flat lamps fabricated by using the optimized $Y_{2.925}Ce_{0.075}Al_{4.79}Si_{0.21}O_{11.72}N_{0.21}$ phosphors with different Si_3N_4 and flux.

Different Si_3N_4 and flux	CIE coordinates		CCT (K)	CRI	Luminous efficacy (lm/W)
	x	*y*			
α-Si_3N_4	0.3489	0.2991	4500	88	42
Nanosized Si_3N_4	0.3685	0.3409	4000	81	58
H_3BO_3	0.3418	0.3388	5100	78	60
NH_4 F	0.3917	0.3804	3700	83	65
LiF	0.3320	0.3116	5500	76	66

3.4. Optical properties of white LED flat source fabricated by the using optimized $Y_{2.925}Ce_{0.075}Al_{4.79}Si_{0.21}O_{11.72}N_{0.21}$ phosphors

Table 5 presents the chromaticity coordinates, the CCTs, the CRI values and the luminous efficacies of the white LED lamps fabricated by using optimized $Y_{2.925}Ce_{0.075}Al_{4.79}Si_{0.21}O_{11.72}N_{0.21}$ phosphors with different Si_3N_4 and flux. The lamps prepared by phosphors doped with nanosized amorphous Si_3N_4 or flux obviously give the enhanced luminous efficacy, e.g. from 42 to 66 lm/W, due to their improved luminescence intensity (Fig. 7a). However, CRI values are correspondingly decreased from 88 to 76 due to the blueshift of emission spectra (Fig. 7b). Therefore, considering the overall optical properties such as CRI and luminous efficacy of LED lamps, NH_4F is a relatively better flux. Under this condition, the white LED lamp fabricated by using a single phosphor shows a CRI as high as 83 and the luminous efficacy is simultaneously enhanced to 65 lm/W under a forward-bias current of 20 mA. Moreover, the chromaticity coordinates of $x = 0.3917$ and $y = 0.3804$ located at the warm white light region and a CCT of 3700 K are also satisfactory for general indoor illuminations.

4. Conclusions

In summary, eminent yellowish orange $Y_{2.925}Ce_{0.075}Al_{5-x}Si_xO_{12-x}N_x$ phosphors were successfully synthesized by a gas-pressure sintering process. When Al^{3+}—O^{2-} pairs are replaced by Si^{4+}—N^{3-} pairs, emission spectra show an obvious redshift and an increase of the FWHM due to the increased covalency and crystal field strength of the host lattice in comparison with typical YAG:Ce garnet phosphors. The blue-light-excitation white LED flat lamp with CRI as high as 88 is realized by using a single oxynitride phosphor with $x = 0.21$. However, the luminous efficacy is significantly decreased because of the decrease of phosphor quantum yield, the worse crystallinity, decreased particle size and irregular morphology. The emission intensity of $Y_{2.925}Ce_{0.075}Al_{5-x}Si_xO_{12-x}N_x$ phosphor can be greatly improved by introducing nanosized amorphous Si_3N_4 or flux. When NH_4F is used as a flux, the white LED lamp fabricated by using a single oxynitride phosphor exhibits an enhanced luminous efficiency of 65 lm/W, a CRI of as high as 83, and a CCT of about 3700 K. These properties are acceptable for general indoor illuminations to replace fluorescent or incandescent light sources.

Acknowledgements

The authors gratefully acknowledge financial supports from National Natural Science Foundation of China (No. 50902050), the Fundamental Research Funds for the Central Universities (No. 78210002), and Special Project for Nanotechnology of Shanghai (No. 11nm0501200).

References

[1] M.S. Shur, A. Zukauskas, Proc. IEEE 93 (2005) 1691–1703.
[2] Y. Uchida, T. Taguchi, Opt. Eng. 44 (2005) 124003-1–124003-9.
[3] A. Katelnikovas, T. Bareika, P. Vitta, T. Jüstel, H. Winkler, A. Kareiva, A. Žukauskas, G. Tamulaitis, Opt. Mater. 32 (2010) 1261–1265.
[4] Q. Li, L. Gao, D. Yan, Mater. Chem. Phys. 64 (2000) 41–44.
[5] Y.P. Fu, J. Alloys Compd. 414 (2006) 181–185.
[6] J.Y. Park, H.C. Jung, G.S.R. Raju, B.K. Moona, J.H. Jeong, S.M. Son, J.H. Kim, Opt. Mater. 32 (2009) 293–296.
[7] H. Bechtel, P. Schmidt, W. Busselt, B.S. Schreinemacher, Proc. SPIE 7058 (2008) 0E.
[8] R. Pazik, P. Głuchowski, D. Hreniak, W. Strek, M. Ros, R. Fedyk, W. Lojkowski, Opt. Mater. 30 (2008) P714–P718.
[9] Y. Narukawa, M. Sano, M. Ichikawa, S. Minato, T. Sakamoto, T. Yamada, T. Mukai, Jpn. J. Appl. Phys. 46 (2007) L963–L965.
[10] A. Michiue, T. Miyoshi, T. Yanamoto, T. Kozaki, S. Nagahama, Y. Narukawa, M. Sano, T. Yamada, T. Mukai, Proc. SPIE 7216 (2009), 72161Z-1.
[11] A.A. Setlur, W.J. Heward, M.E. Hannah, U. Happek, Chem. Mater. 20 (2008) 6277–6283.
[12] H.S. Jang, W.B. Im, D.C. Lee, D.Y. Jeon, S.S. Kim, J. Lumin. 126 (2007) 371–377.
[13] Y. Pan, M. Wu, Q. Su, J. Phys. Chem. Solids 65 (2004) 845–850.
[14] T. Moriga, Y. Sakanaka, Y. Miki, K.I. Murai, I. Nakabayashi, Int. J. Mod. Phys. B 20 (2006) 4159–4164.
[15] K. Li, G. Shucai, H. Guangyan, Z. Jilin, J. Rare Earth 25 (2007) 692–696.
[16] C.C. Chiang, M.S. Tsai, M.H. Hon, J. Alloys Compd. 431 (2007) 298–302.
[17] H. Yang, D.K. Lee, Y.S. Kim, Mater. Chem. Phys. 114 (2009) 665–669.
[18] Y.Q. Li, J.E.J. van Steen, J.W.H. van Krevel, G. Botty, A.C.A. Delsing, F.J. DiSalvo, G. de With, H.T. Hintzen, J. Alloys Compd. 417 (2006) 273–279.
[19] H.L. Li, R.J. Xie, N. Hirosaki, Y. Yajima, J. Electrochem. Soc. 155 (2008) J378–J381.
[20] R.J. Xie, N. Hirosaki, K. Sakuma, Y. Yamamoto, M. Mitomo, Appl. Phys. Lett. 84 (2004) 5404–5406.
[21] H.L. Li, R.J. Xie, N. Hirosaki, T. Suehiro, Y. Yajima, J. Electrochem. Soc. 155 (2008) J175–J179.
[22] K. Uheda, N. Hirosaki, Y. Yamamoto, A. Naito, T. Nakajima, H. Yamamoto, Electrochem. Solid State Lett. 9 (2006) H22–H25.
[23] H. Watanabe, H. Yamane, N. Kijima, J. Solid State Chem. 181 (2008) 1848–1852.
[24] G. Blasse, B.C. Grabmaier, Luminescent Materials, Springer, Berlin, 1994.
[25] A. Katelnikovas, H. Bettentrup, D. Uhlich, S. Sakirzanovas, T.J. üstel, A. Kareiva, J. Lumin. 129 (2009) 1356–1361.
[26] M.C. Maniquiz, K.Y Jung, S.M. Jeong, J. Electrochem. Soc. 157 (2010) H1135–H1139.
[27] A.A. Setlur, E.A. Bachniak, U.S. Patent Application 2006/0197443, 2006.
[28] Y.S. Lin, Y.H. Tseng, R.S. Liu, J.C.C. Chan, J. Electrochem. Soc. 154 (2007) P16–P19.
[29] T. Fiedler, T. Fries, F. Jermann, M. Zachau, F. Zwaschka, World Patent WO2005/061659A1, 2005.
[30] P.J. Schmidt, W. Mayr, J. Meyer, B. Schreinemacher, World Patent WO2006/095284A1, 2006.
[31] W.Y. Sun, X.T. Li, L.T. Ma, T.S. Yen, J. Solid State Chem. 51 (1984) 315–320.
[32] E. Zych, A. Walasek, J. Alloys Compd. 451 (2008) 582–585.
[33] A.A. Setlur, A.M. Srivadtava, Opt. Mater. 29 (2007) 1647–1652.
[34] G. Wyszecki, W.S. Stiles, Color Science: Concepts and Methods, Quantitative Data and Formulae, 2nd ed., John Wiley & Sons, New York, 1982.